energies

MDPI

Article

Multi-Physics Tool for Electrical Machine Sizing

Yerai Moreno [1,*], Gaizka Almandoz [1], Aritz Egea [1], Patxi Madina [1] and Ana Julia Escalada [2]

[1] Faculty of Engineering, University of Mondragon, 20500 Mondragon, Spain; galmandoz@mondragon.edu (G.A.); aegea@mondragon.edu (A.E.); pmadina@mondragon.edu (P.M.);
[2] ORONA EIC, 20120 Hernani, Spain; ajescalada@orona-group.com
* Correspondence: yerai.moreno@alumni.mondragon.edu

Received: 17 February 2020; Accepted: 26 March 2020; Published: 2 April 2020

Abstract: Society is turning to electrification to reduce air pollution, increasing electric machine demand. For industrial mass production, a detailed design of one machine is usually done first, then a design of similar machines, but different ratings are reached by geometry scaling. This design process may be highly time-consuming, so, in this paper, a new sizing method is proposed to reduce this time, maintaining accuracy. It is based on magnetic flux and thermal maps, both linked with an algorithm so that the sizing process of an electrical machine can be carried out in less than one minute. The magnetic flux maps are obtained by Finite Element Analysis (FEA) and the thermal maps are obtained by analytical models based on Lumped Parameter Circuits (LPC), applying a time-efficient procedure. The proposed methodology is validated in a real case study, sizing 10 different industrial machines. Then, the accuracy of the sizing tool is validated performing the experimental test over the 10 machines. A very good agreement is achieved between the experimental results and the performances calculated by the sizing tools, as the maximum error is around 5%.

Keywords: sizing methodology; electrical machines; thermal model; electromagnetic model; permanent magnet

1. Introduction

Society is turning to electrification in transportation and industrial processes to reduce emissions, embrace alternative energy, and increase efficiency. In this regard, permanent magnet synchronous machines (PMSM) are mostly used for traction applications, due to their high power density and high efficiencies [1].

However, the main drawback of PMSM and electrical machines in general is their complex and time-consuming design process, as different targets must be reached optimizing various parameters that are cross-coupled. Usually, the final objective of the design is to minimize the cost of the machine while maximizing its efficiency. To fulfill these objectives coping with the growing machine demand, the design process must be improved.

Once the design requirements are defined, there are two designing scenarios, one where the machine is designed from scratch and another one where a 2D computer-aided design plane (2D CAD) is selected from the ones previously designed and the machine is sized setting the appropriate stack length and number of turns for the specific application. Different magnets and sheet types can be also chosen. Usually, in a company with a wide range of electric machines, the second scenario could be more usual, making it more competitive in the market, as the process is faster than designing a machine from zero. In addition, keeping the same electric sheets and the same motor concept reduces the manufacturing cost considerably, as the same manufacturing process can be used for building a wide range of electrical machines.

In this paper, the second scenario is analyzed, where the stator and rotor sheets are selected from a 2D plane database, and after the machine is sized. In Figure 1a, the general process is shown.

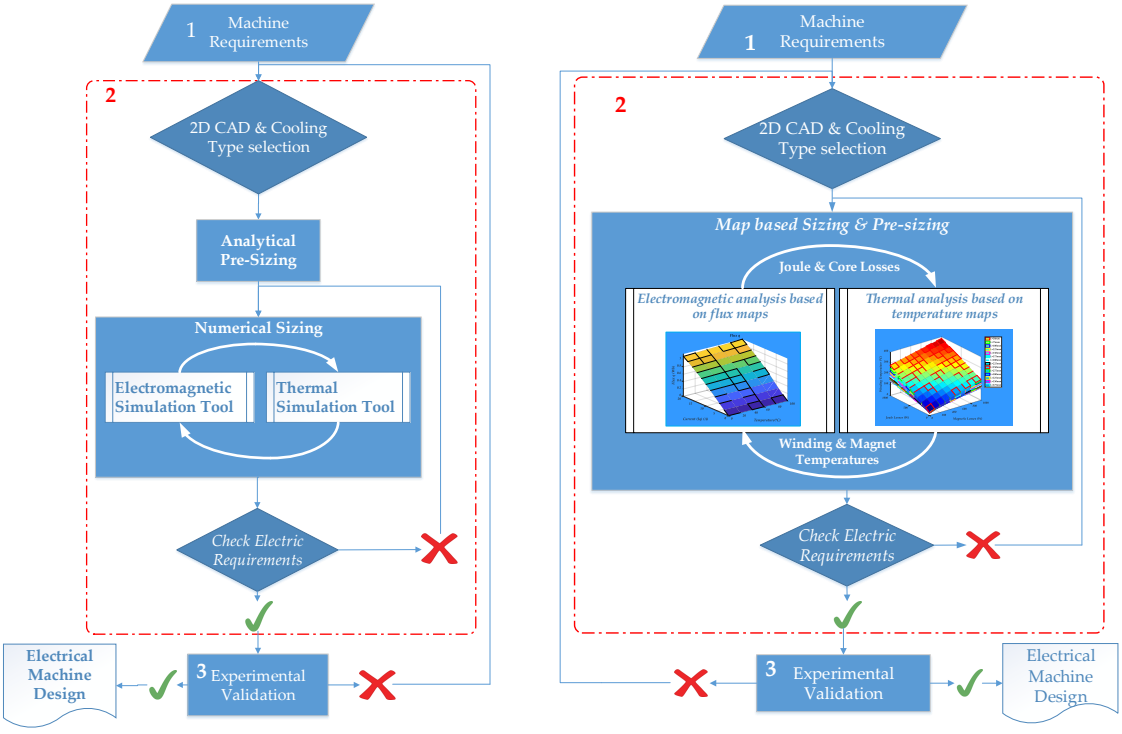

(**a**) (**b**)

Figure 1. Description of the sizing methodology using multi-physics tool. (**a**) classical Method; (**b**) integration of the sizing multi-physics tool in the classical method.

Firstly, machine requirements must be defined (1) including working currents, voltages, application temperature, output torque, and speed. These technical requirements come from the customer functional specifications that must be precise, as the design is optimum for the application.

Secondly, the machine is sized (2). The optimum 2D plane and cooling type must be selected for the application. Then, an analytical pre-sizing is made, to have an approximate number of turns, and stack length, together with the wire section. Next, the main step of the sizing process starts, using electromagnetic simulation tools together with thermal ones, to make a more accurate calculation of the machine. Lastly, the obtained performances are automatically checked, and if the machine does not comply the requirements, changes are made to the stack length or the number of turns, making the calculation again, until the design fulfills the requirements.

Finally, the machine is validated experimentally in (3) to check that the machine performance is equal to the simulated one. If the bench test is correct, the sizing of the machine is achieved; otherwise, the process must start again from the beginning.

As mentioned before, PMSM is the most used electric machines for traction, and one of their main characteristics is the nonlinearity, as well as their temperature dependences in the generated magnetic flux. They can also get demagnetized if they continuously suffer thermal overload [1–3]. This is why electromagnetic simulations must be linked to thermal ones, making them more accurate as a whole. However, linking the two simulations causes a longer iterative process, increasing the computational and design time.

To avoid this, a map interpolation is proposed, to obtain magnet and copper temperature based on Joule and Core losses. It will obtain the steady-state temperatures by a fast iteration taking into account loss change with temperature. Finally, working temperature performances can be obtained with a new magnetic flux interpolation and some simple calculations.

With respect to electromagnetic simulations, there are different tools to make it, with diverse accuracy and time consumption ranks—for instance, analytic equations, lumped parameter models, Fourier series models, and Finite Element Analysis (FEA).

The fastest way of sizing a machine is using fundamental machine sizing equations as shown in [4,5]. This analytical method is mostly used for preliminary machine sizing, in the first stages of the process due to its speed. Nevertheless, it does not provide a high accuracy compared to FEA solutions.

Another analytical method is the one based on Fourier series. In this case, the accuracy and computational time depend on the number of spatial harmonics considered in the different machine regions. The higher the harmonic orders are, the higher the accuracy is, but the longer time the computation takes. If magnetic saturation plays an important role in the designed machine, this method should be avoided using FEA, where local magnetic saturation may be considered [6].

With the aim to be more accurate, Lumped-Parameter (LP) models are developed. This method takes into account magnetic saturation and it can be more accurate than other analytical methods, still being faster than FEA. However, the more accurate is the result, the slower is the calculation, so the equilibrium between speed and accuracy is the key [1].

FEA is considered the standard tool for electric machine analysis, as it has a detailed magnetic field solution, including saturation, providing an accurate result of the machine performance according to the density of the mesh. Despite this, FEA needs a massive computational effort and time consumption [7].

In order to reduce FEA computation time maintaining its accuracy, different methods are found in the literature that mix initial FEA simulations with different scaling methods to size different machines. In [8,9], dimensional and number of turns scaling techniques are used after a base machine FEA simulation is carried out. This simulation generates magnetic flux, loss, and torque maps that are used to generate other machine models with the mentioned scaling techniques. For instance, second-order polynomial functions are used in [3] to describe magnetic flux linkage variations respect to current, using FEA models just to calculate parameters of the functions. Then, combined with other analytical models, other machines can be sized based on the reference. Moreover, in [10], FEA is also combined with analytical models to obtain a rapid tool of induction machine mapping in dq axes. The results of these methods are rather accurate, as they are based on FEA models.

As mentioned before, the thermal model must also be simulated, to evaluate working temperatures and their distribution along the machine, linking it to the electromagnetic model. As in electromagnetic calculations, there are various methods with different performances such as FEA, LP models, and Computational Fluid Dynamic (CFD), shown in [11,12].

As in the previous case, the objective is to simulate as accurately and as quickly as possible. The speediest way is to simulate the machine with LP thermal networks as they are quite accurate as shown in [4,13], but they can become as slow as FEA if many nodes are introduced. Therefore, some reduced node models are found in literature, reducing computation time considerably, maintaining good accuracy [14,15].

Gaining accuracy, there is CFD software, used for modelling cooling systems, calculating flow rates, and heat transfer. The main asset is that it can be used to predict the flow in complex regions, such as around the end windings, with great precision. Moreover, the data obtained from CFD can be used to improve analytical algorithms in analytic thermal networks. However, its big disadvantage is its huge computation needs and time consumption, making it unsuitable for fast sizing process, but might be used in big machines with a high cost of prototypes [11,12].

In thermal modelling, FEA is used to accurately calculate the conduction heat transfer in complex geometric shapes, such as heat transfer through strands of copper in a slot. Nevertheless, it has an important limitation as the software uses analytical/empirical-based algorithms for convection boundaries, exactly as in the lumped circuit analysis. As a result, the accuracy is dependent on the same factors for the thermal network; just making a difference when the solid component conduction must

be calculated precisely. Some authors used a 3D reduced-order FEA model to reduce computational time maintaining a rather good accuracy [2,11].

Taking into account all the simulation methods found in literature, magnetic flux and temperature maps are used in the proposed sizing method. Magnetic flux maps are obtained from FEA simulations and temperature maps are generated from lumped parameter network simulations. In this way, a fast and accurate method can be defined.

In this article, a fast sizing method is proposed. It sizes a machine in about one minute, maintaining the accuracy of the Finite element models. The major novelty of this method is the coupling between thermal and electromagnetic fields. The sizing is done by an iterative algorithm.

Finally, the proposed method is validated in a real case study, sizing 10 industrial machines used for people transportation systems.

This paper is organized as follows: Section 2 describes the proposed method and explains the theoretical base of the method. The initial simulation process and the sizing algorithm are presented. Section 3 compares the obtained data with 10 industrial machine experimental results to validate the algorithm and the proposed process. In Section 4, the novelty of the work is presented, with the obtained results and their conclusions.

2. Description of the Proposed Sizing Procedure

In this section, the procedure for obtaining the magnetic flux maps and the thermal maps is explained. As it is shown in Figure 2, this procedure consists of two different simulations. Magnetic flux maps are obtained by electromagnetic FEA simulations performed using Altair Flux® (Troy, MI 48083, USA), whereas the temperature maps are obtained by thermal simulations carried out using Motor-CAD® (Wrexham LL13 7YT, UK).

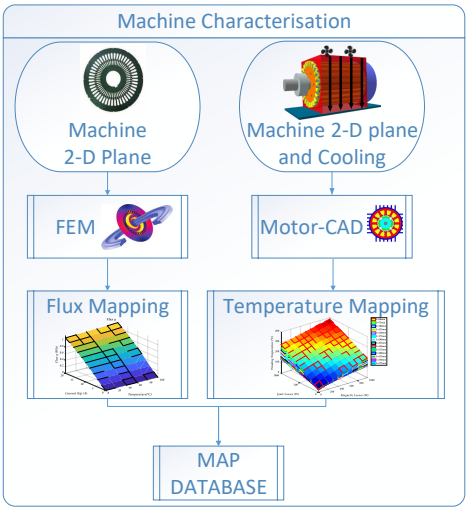

Figure 2. Map database creation.

Concerning the magnetic flux maps, d-q axis magnetic flux is computed as a function of d-q axis currents and magnet temperature. Regarding the temperature maps, two maps are obtained as well—one map for the average winding temperature and another one for the average magnet temperature. Both maps are computed as a function of the Joule and magnetic losses, accounting for different stack lengths.

These maps make up a database in which different magnetic circuit 2D geometries and cooling types are included. This way, during the sizing process of electrical machines, different magnetic flux and temperature maps are used according to the chosen 2D geometry of the lamination and the cooling solution. In the next sections, more details are given about the map creation procedure.

2.1. Magnetic Flux Map Creation

D-Q axis magnetic flux maps are obtained performing FEA magneto-static simulations. As the electrical machine analysis involves magnetic and electric domains, the magnetic circuit of the motor is coupled to the electric circuit.

In case the machine geometry is simple, FEA 2D simulations could be suitable. However, complex motor geometries might require FEA 3D simulations. The proposed procedure in this paper is suitable for both cases, FEA 2D and FEA 3D.

The objective is to generate magnetic flux maps depending on current (in d-q axis) and temperature, so $\varphi_q\left(i_q, i_d, T_{magnet}\right)$ and $\varphi_d\left(i_q, i_d, T_{magnet}\right)$ are obtained. As the map depends on three variables, magnet temperature, d, and q currents, many simulations must be performed varying these three variables.

The first step is to define the currents and temperature variation ranges to generate the solving scenario for the model, as shown in Figure 3.

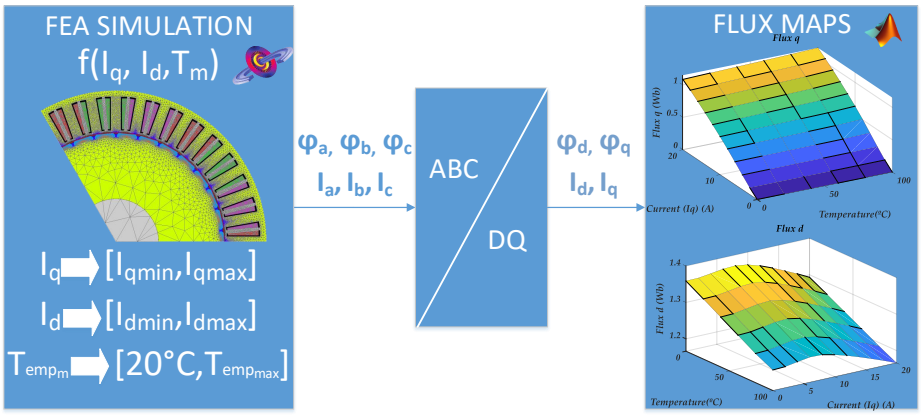

Figure 3. Magnetic flux map generation process.

One criterion for defining the currents' variation range could be the saturation of the magnetic material. For instance, for a given N, the maximum supplying current value could be defined according to the linearity of the q axis magnetic flux as a function of the q axis current, from 0 A up to the point at which the linearity of the q axis magnetic flux decrease in a given value. The effect of the magnet temperature is accounted for changing the remanence value of the magnets field. The maximum value of the remanence value can be set according to the standard data-sheets of commercial magnets. For instance, nowadays, the maximum remanence field that can be found in the market for Neodymium magnets is around 1.43 T (N52M from Baker Magnetics (5692 Elson, The Netherlands)). Concerning the minimum remanence value, it could be defined also considering standard properties of the magnets in the market. For example, a suitable criterion could be to consider the minimum remanence value at room temperature around 0.98 T (N25 BH from Baker Magnetics) and compute the remanence value at the maximum working temperature of the same magnet, about 240 °C. Applying this criterion, the magnet remanence value should be varied in the range of 0.74 T–1.43 T.

It is also important to define NI properly, to obtain data in the machine working range. If a working point of a machine exceeds the maximum value of the map range, the map will not be suitable for sizing the desired machine because it would need to extrapolate and extrapolation may generate incorrect results.

Flux® software performs the electromagnetic analysis solving Maxwell's equations with a magnetic vector potential, finally solving Equation (1) by finite element methods:

$$\nabla \times \left(v_0 \left[v_r \right] \nabla \times \vec{A} \right) + \left[\sigma \right] \left(\frac{\partial \vec{A}}{\partial t} + \nabla V \right) = 0 \tag{1}$$

where $[v_r]$ is the tensor of the reluctivity of the medium, v_0 is the reluctivity of the vacuum, $\overrightarrow{A}$ is the magnetic vector complex potential, $[\sigma]$ is the tensor of the conductivity of the medium, and V is the electric scalar potential.

Once the solving scenario is defined, the simulation is carried out to get $\varphi_a \left(i_q, i_d, T_{magnet} \right)$, $\varphi_b \left(i_q, i_d, T_{magnet} \right)$ and $\varphi_c \left(i_q, i_d, T_{magnet} \right)$. Then, these variables are post-processed to get $\varphi_q \left(i_q, i_d, T_{magnet} \right)$ and $\varphi_d \left(i_q, i_d, T_{magnet} \right)$. This will be done with Clark–Park transformation [16], as shown in the second step of Figure 3. Finally, the obtained magnetic fluxes shown in Figure 3 will be saved in a magnetic flux map database for future use.

The resolution of the maps must be properly chosen as it might affect the accuracy of the final results given by the sizing tool. Defining at least 10 computation points in the variation range of each variable could be a criterion. This leads to at least 1000 different simulations to be performed by FEA. Another key point affecting the accuracy is the resolution of the simulations. A criterion could be to consider at least 100 points in a single electric period, so 100 points are performed for each simulation, leading to a total amount of 100,000 simulation points. Using an average computer (16 GB RAM, 64 bytes—3.41 GHz Microprocessor), the solving of a single point could take around 5 s, leading to a total simulation period of five days. It might not be too much considering that the magnetic flux maps are obtained once and then no more FEA simulations are required for a given magnetic circuit geometry. Nevertheless, in case the data-sheet must be made-up with many different magnetic circuit geometries, this task could take a lot. Thus, in this paper, a proposal is presented to reduce the computation load of the magnetic flux mapping process.

As shown in Figure 4, during one full electric period of φ_a, φ_b, and φ_c, there are six φ_d periods, so it is enough to simulate 1/6 of the period to obtain φ_d, reducing significantly the computation time.

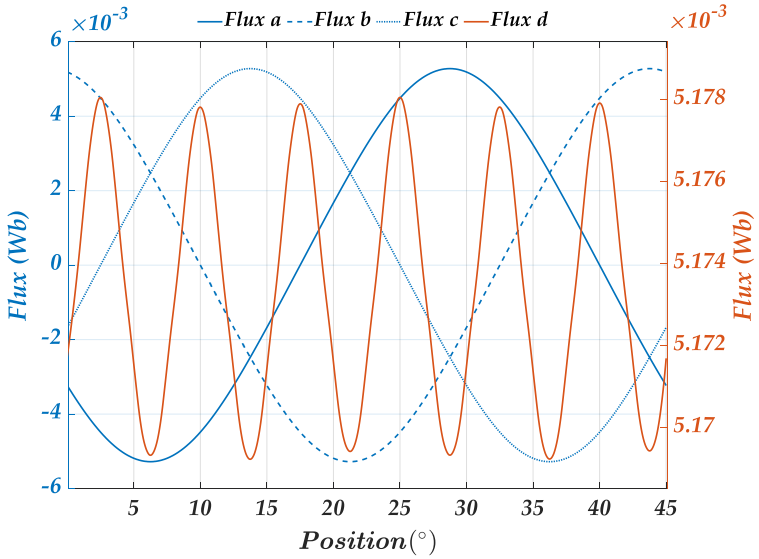

Figure 4. Magnetic fluxes during a full electrical period.

2.2. Temperature Map Generation

As mentioned in Section 1, there are different methods and software to model the thermal performance of electrical machines. In this paper, the commercial software Motor-CAD® is used to obtain the required temperature maps.

Motor-CAD® uses a three-dimensional lumped circuit model that can be used to calculate the steady-state and transient thermal characteristics of several motor types. One of the most complex aspects of motor thermal analysis is the prediction of Convection Heat Transfer mainly relating to the outer surface of the motor, but also for the internal air-gap. An estimation is made by the software using natural and forced convection correlations. Radiation Heat Transfer is also modelled in Motor-CAD.

The process for obtaining these maps is shown in Figure 5. First, the model is defined, using the stack 2D plane and the desired cooling system, generating the thermal network.

Average winding temperature and average magnet temperature maps are obtained as a function of the Joule and Magnetic losses and accounting for different stack lengths. The variation range for the losses and the stack length must be properly established to assure that all thermal situations demanded during the sizing process are covered by the maps.

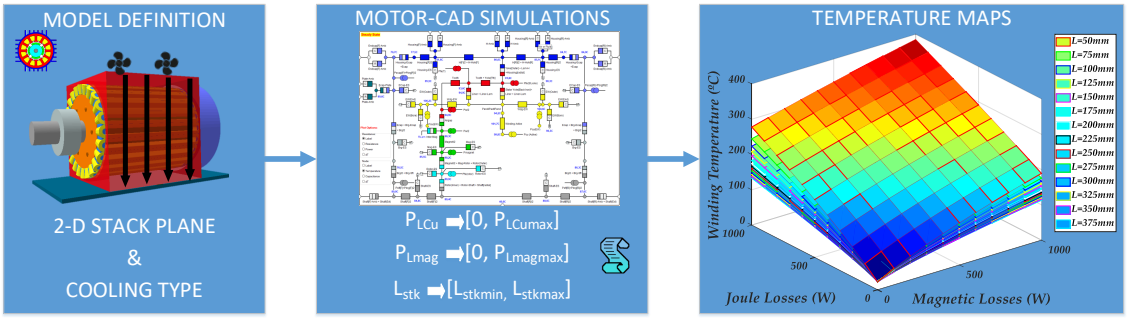

Figure 5. Temperature map generation.

The variation range and the resolution of the stack length will be defined by the user.

The variation range of the losses could be established accounting for the winding temperature. For instance, it does not make sense to consider losses that raise the temperature above the maximum limit for the maximum stack length (keeping the losses constant, the smaller the stack length is, the higher the temperatures are. Thus, for small stack lengths, the temperatures might lead above the maximum limit).

This way, the variation range of the losses and the stack length should be defined for every particular case. The model is simulated for each defined point of power losses and length combination. One of these simulations is done for each cooling type.

Finally, temperature maps are created. $T_{\text{magnet}}\left(P_{\text{LCu}}, P_{\text{Lmag}}\right)$ and $T_{\text{Cu}}\left(P_{\text{LCu}}, P_{\text{Lmag}}\right)$ maps are shown in next Section 3, Section 3.2. Each layer represents one stack length, from the smallest machine in the upper layer, to the longest in the lower (and coldest) layer.

2.3. Sizing Method

In this section, the proposed sizing process of electrical machines is described. As it is shown in Figure 6, before the sizing process begins, the design requirements must be defined. Then, the cooling solution and the 2D magnetic circuit geometry must be chosen. Once these two elements are chosen, the corresponding magnetic flux and temperature maps are uploaded to the sizing program. As it can be appreciated in Figure 6, the sizing process consists of three main stages:

- STAGE 1: DEFINITION OF L & Z. At the first step, preliminary values for the number of turns and the stack length are estimated. Then, if after the calculations the checking is not correct, L

& Z will be recalculated. Depending on the obtained performances, L & Z values will increase or decrease.

- STAGE 2: ELECTROMAGNETIC & THERMAL ANALYSIS. With the defined L & Z, dq magnetic fluxes are obtained by the interpolation on the magnetic flux maps. Then, machine performances are calculated, such as Joule and magnetic losses. These losses will be used to obtain the working temperature of the winding and the magnets by interpolating in the temperature maps. With the working temperatures, performances are calculated again, based on a new magnetic flux map interpolation. At the end of this process, performances of the machine are obtained at ambient and working temperatures.
- STAGE 3: AUTOMATIC CHECKING. The performances are checked and, depending on the results, the process is finished or a new iteration is started returning to Stage 1.

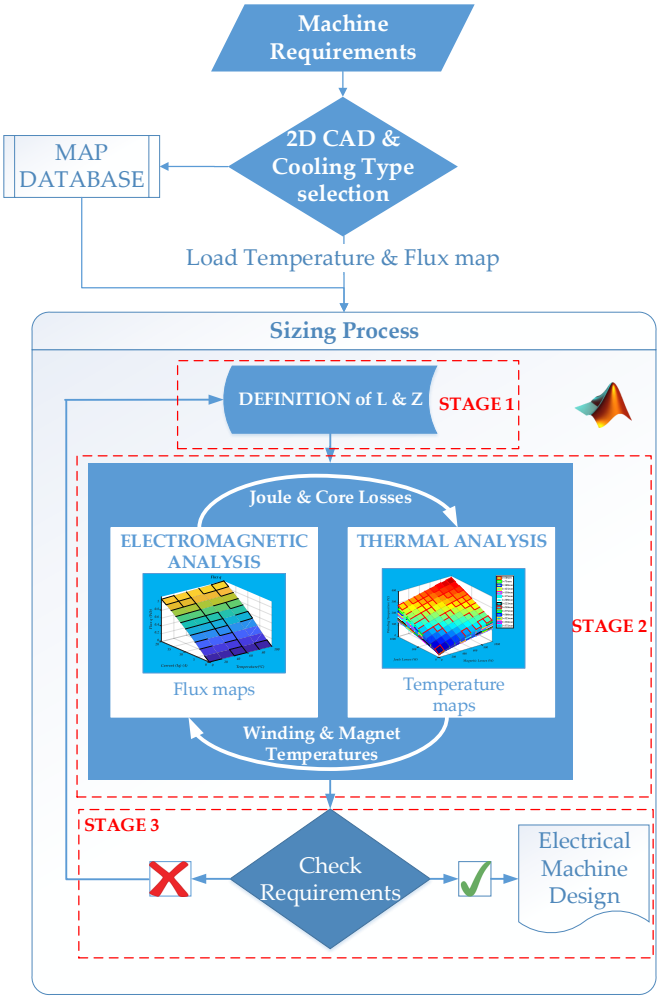

Figure 6. Sizing algorithm.

2.3.1. Stage 1: Definition of L & Z

Once the main design requirements are defined, the number of turns and the stack length are pre-calculated considering the torque Vs current requirement, and the voltage limitation, applying the next well known torque and voltage analytical Equations (2):

$$\begin{cases} T_{\text{nom}} = 3p\varphi_{\text{d}} L N I_{\text{n}} \\ V_{\text{max}}^2 = \left(-\varphi_{\text{q}} + N^2 L k_{\text{ov}} w_{\text{e}} I_{\text{n}}\right)^2 + \left(2\rho N^2 n_{\text{cap}} I_{\text{n}} \frac{L+L_{\text{end}}}{A_{\text{r}} k_{\text{f}}} + \varphi_{\text{d}} N L w_{\text{e}}\right)^2 \end{cases} \tag{2}$$

where T_{nom} is the nominal torque (Nm), p is the machine pole pairs, φ_{d} is magnetic flux d (Wb), φ_{q} is magnetic flux q (Wb), L is the machine stack length (m), N is winding number of turns, I_{n} is the desired nominal current (A), V_{max} is the maximum allowed voltage (V), k_{ov} is the overlapping factor, w_{e} is the machine rotational speed (rad/s), ρ is the wire resistivity (Ωm), n_{cap} is the number of winding layers, L_{end} is the end-winding length (m), A_{r} is the copper wire area (m^2), and k_{f} is the filling factor.

Solving the equation system (2), the initial length and number of turns are estimated, providing an accurate starting point of the iterative loop, instead of traditional iteration starting from a particular point every time. Overlapping and filling factor values for the estimation are fixed, but they could be adjusted depending on the number of turns and the final chosen wire section.

2.3.2. Stage 2: Electromagnetic & Thermal Analysis

Once initial number of turns (N_{ini}) and initial stack length (L_{ini}) are defined, it is time to interpolate in the magnetic flux map. At the first iteration, ambient temperature is taken for the interpolation. Nominal current is set to obtain the required torque, interpolating and obtaining φ_{d} and φ_{q}.

The interpolated value at a query point is based on linear interpolation of the values at neighbouring grid points in each respective dimension. This method is accurate enough if the map resolution is properly defined. Extrapolation is not recommended as it may result in false values of magnetic flux or temperature in case of thermal maps.

For resistance calculation, standard values of wire diameter are tabulated for each number of turns, to obtain a suitable filling factor depending on the chosen winding type, p.e. around 0.42 for distributed windings and around 0.5 for concentrated windings. The overlapping factor is defined with an experimentally adjusted curve. With this data and motor geometry, end-winding length (L_{end}) is calculated with (3), finally obtaining winding resistance (R_{Cu}) with (4), where ρ is copper resistivity at 20 °C. Moreover, q axis inductance is calculated by definition in (5):

$$L_{\text{end}} = \frac{\frac{\pi}{2}\left(\frac{D\pi}{Q_{\text{s}}} + w_{\text{d}}\right) * k_{\text{ov}}}{1000} \tag{3}$$

where D is stator diameter, Q_{s} is the number of slots, w_{d} is the slot width, and k_{ov} is the overlapping factor:

$$R_{\text{Cu}} = \frac{\rho(L_{\text{end}} + 2L)(1 + 0.0039(T_{\text{Cu}} - 20))}{A_{\text{r}}} \tag{4}$$

$$L_{\text{q}} = \frac{\varphi_{\text{q}}}{i_{\text{q}}} \tag{5}$$

Then, voltage is calculated, as shown in (6), where V_{d} and V_{q} are dq voltages, and L_{σ} is the leakage inductance:

$$\begin{cases} V_{\text{d}} = R_{\text{Cu}} i_{\text{d}} - L_{\sigma} w_{\text{e}} i_{\text{q}} - \varphi_{\text{q}} w_{\text{e}} \\ V_{\text{q}} = R_{\text{Cu}} i_{\text{q}} + L_{\sigma} w_{\text{e}} i_{\text{d}} + \varphi_{\text{d}} w_{\text{e}} \end{cases} \tag{6}$$

Finally, losses are calculated. Joule losses are calculated by Joule's law (7), while Core losses are calculated with the Bertotti's Model (8) shown in [17]:

$$P_{\mathrm{LCu}} = 3R_{\mathrm{Cu}}I^2 \tag{7}$$

$$\begin{cases} p_{\mathrm{Fe}} = p_{\mathrm{h}} + p_{\mathrm{c}} + p_{\mathrm{e}} = k_{\mathrm{h}} f B_{\mathrm{s}}^{\alpha} + \sum_i k_{\mathrm{c}} f^2 B_{\mathrm{si}}^2 + \sum_i k_{\mathrm{e}} f^{1.5} B_{\mathrm{si}}^{1.5} \\ P_{\mathrm{Fe}} = k_{\mathrm{a}} p_{\mathrm{Fe}} W_{\mathrm{m}} \end{cases} \tag{8}$$

where p_{Fe} is the core loss per weight, p_{h} is the hysteresis loss, p_{c} is the eddy current loss, p_{e} is the excess loss, k_{h} is the hysteresis loss coefficient, k_{c} is the eddy current loss coefficient, k_{e} is the excess loss coefficient, α is an Steinmetz coefficient, f is the frequency, B_{si} is the i^{th} harmonic amplitude of the stator magnetic flux density, k_{a} is the empirical coefficient, and W_{m} is the weight of motor.

Once Joule and Core losses are obtained at working temperature, they are sent to the thermal analysis. Then, the first interpolation can be made in the temperature maps, obtaining winding and magnet temperatures. Nevertheless, these temperatures are not the steady-state ones; as with temperature change, losses also change. To obtain the steady-state working temperatures, Joule losses are updated with temperature, as the resistance varies with temperature. The thermal analysis block will make this iteration until the steady-state losses and temperatures are obtained, taking about 16 iterations.

Once steady-state temperatures are obtained, they are returned to the electromagnetic analysis block, so the performances are obtained at working temperatures.

2.3.3. Stage 3: Automatic Checking

After obtaining the electrical performances at room and working temperatures, they must be checked, and, if they fulfil all the requirements, the sizing process will be finished, generating a favourable machine design report. Otherwise, the design parameters are changed and the calculus is addressed again. Figure 7 shows which parameters are checked, and the actions adopted (in STAGE 1) if they are not fulfilled. In the figure, L+ refers to increasing the machine length in one step, and Z+ or Z− means increasing or decreasing conductors in each slot.

Checking minimum voltage is interesting, but it is not mandatory as some machines will not be able to fulfill both maximum and minimum voltages.

This checking is made automatically with the proposed algorithm taking into account designer specifications as the minimum and maximum voltages, maximum current, and maximum temperatures.

These requirements are set by the designer at the beginning of the process. The maximum voltage and current usually are limited by the inverter or the grid and the winding temperature normally is limited by the material or the machine class. If just one of the parameters does not comply, changes are made and another iteration is made, checking the four parameters again at its end. If all parameters are fulfilled, this is the optimum length and number of turns for the machine so the report is favourable, ending the process.

A Graphic User Interface (GUI) is designed to implement the proposed method in an easy and user-friendly way, to save time and effort when sizing machines. This GUI is composed of a database containing magnetic flux and temperature maps, an interface to choose those maps and introduce design requirements, a calculation core to implementing the proposed algorithm and a report generator to show the results after the results are automatically checked.

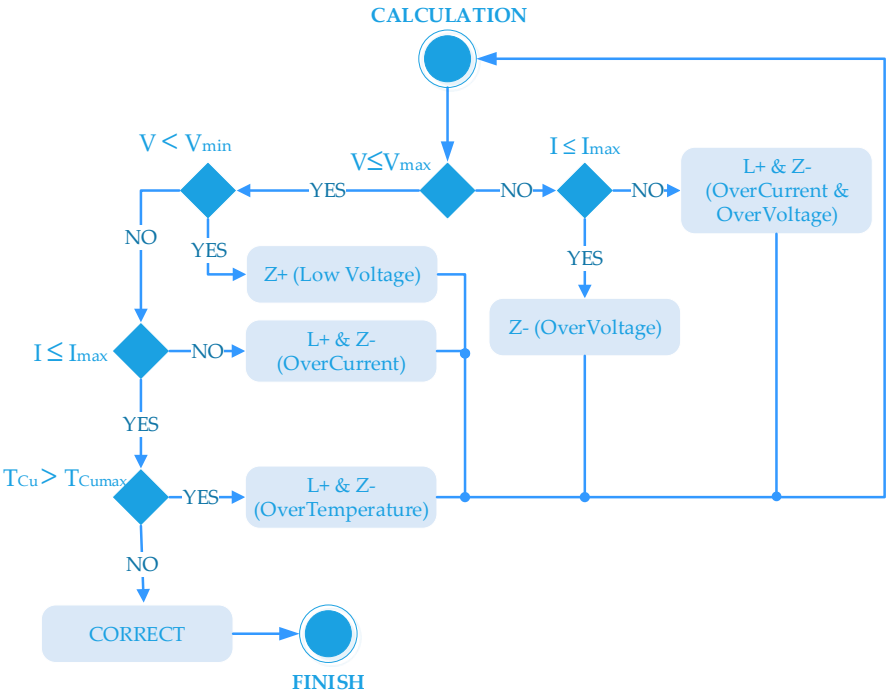

Figure 7. Automatic checking process after each iteration.

3. Case Study: Sizing of PMSM for People Transportation

In this section, the proposed improved sizing methodology is implemented in a real case study. The objective is to validate the multi-physics tool sizing several commercial PMSM for people transport application.

3.1. Description of the Machines

These machines are based on conventional topology comprising 36 slots in the stator and 30 poles in the rotor (Qs36p15). In total, ten different machines have been sized by the proposed method and tested experimentally. Their performances are shown in Table 1.

Table 1. Main machine performances

Motor ID	Speed [rpm]	Nominal Torque [Nm]	Power [kW]	Stack Length [mm]
M1	200	100	2.1	100
M2	400	100	4.2	100
M3	200	200	4.2	125
M4	400	200	8.4	125
M5	200	300	6.3	175
M6	400	300	12.6	175
M7	200	400	8.4	225
M8	400	400	16.7	225
M9	200	500	10.5	300
M10	400	500	21	300

In Figure 8, the stator and the rotor corresponding to one of the tested motors, and the ID 5 are shown.

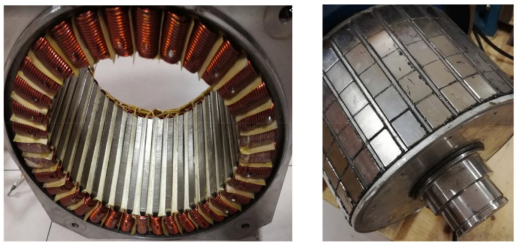

Figure 8. Rotor and Stator of one motor experimentally tested (Motor ID 5).

3.2. Map Creation

All of the tested machines have the same 2D magnetic circuit shown in Figure 9. The active length and the number of turns per phase are adjusted to fulfill the requirements of each application.

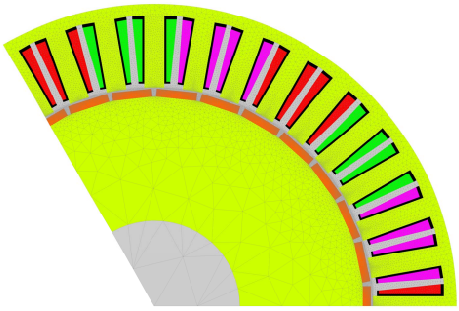

Figure 9. Geometry of the sized machines (Qs36p15).

In this case, the tested motors have surface-mounted permanent magnets and concentrated windings. In the future, the multi-physics sizing tool can be used with interior magnet motors or distributed windings to broaden the validation.

As mentioned in Section 2, magnetic flux maps must be created for each 2D geometry, generating the maps shown in Figure 10. Figure 10a shows magnetic flux in the d axis, whereas Figure 10b shows magnetic flux in the q axis.

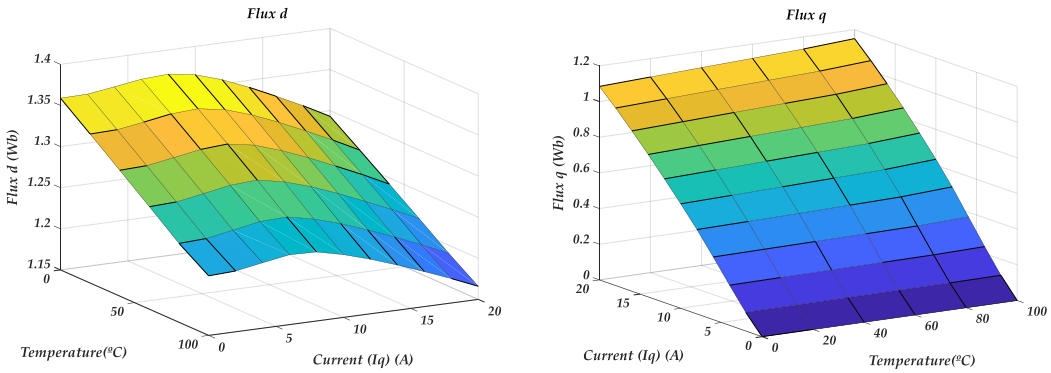

(**a**) (**b**)

Figure 10. Generated magnetic flux maps: magnetic flux vs. Current and Temperature for the Qs36p15 motor. (**a**) D magnetic flux map; (**b**) Q magnetic flux map.

As it can be appreciated in Figure 10, the temperature mainly affects to the d-axis magnetic flux because the remanent field of the magnets decreases linearly as the temperature increases. On the contrary, the q-axis magnetic flux changes slightly with the temperature. In this case, these small

variations are due to changes in the saturation of the magnetic circuit. The magnetic flux created by the magnets changes with the temperature leading to variations in the saturation.

Ideally, in universal d-q axis models of the PMSM, it is commonly considered that the d-axis magnetic flux depends on the magnet flux and the d-axis current, while the q-axis magnetic flux depends only on the q-axis current. Nevertheless, there might be a fairly cross-coupling effect between the d-q axis depending on the saturation level of the motor, which might lead to relevant errors in the final results. In this case, this cross-coupling effect is clearly appreciated in Figure 10a as the d-axis magnetic flux changes with the q-axis current. In addition, this relationship is not linear, which makes it more difficult to model. Interpolating the magnetic flux maps, as it is done in the proposed tool, all these nonlinearities are taken into account, making it possible to achieve accurate results to some extent.

With respect to thermal maps, the Q36p15 motor model is shown in Figure 11. This model is used to create the maps, with the geometry and the selected cooling system—natural convection in this case.

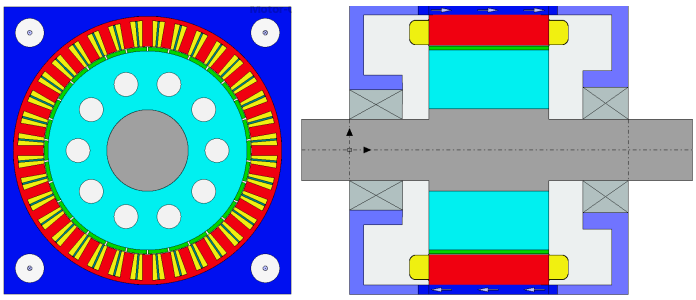

Figure 11. Motor-CAD® Model of the sized machines.

As mentioned in Section 2, temperature maps must also be created for each 2D geometry and cooling type, generating the maps shown in Figure 12. Figure 12a shows the mean winding temperature, whereas Figure 12b shows the mean magnet temperature. As it can be seen, shorter machines get warmer easier, and they will tolerate lower losses. In conclusion, if a machine exceeds the maximum desired temperature of the winding, or the demagnetization temperature of the magnets, a longer machine may be chosen.

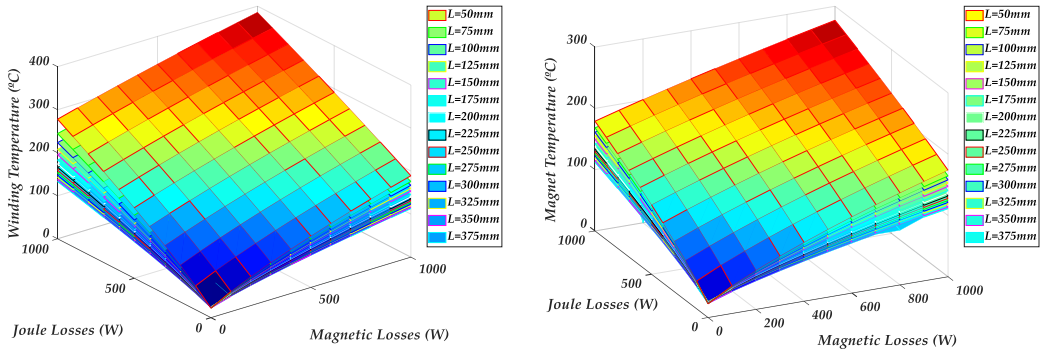

(**a**) (**b**)

Figure 12. Generated Temperature maps: Temperature vs. Magnet Losses, Copper Losses and Stack length in the naturally cooled machine with Qs36p15 configuration. (**a**) winding temperature map; (**b**) magnet temperature map.

3.3. Sizing

In Figure 13, sizing results are shown. It can be seen that most of the machines have the same EMF constant, as it was expected. In addition, voltage trends are very similar between machines,

although some of them reach slightly higher voltage values. The figure also shows that machines are more efficient at nominal currents than at low and high currents.

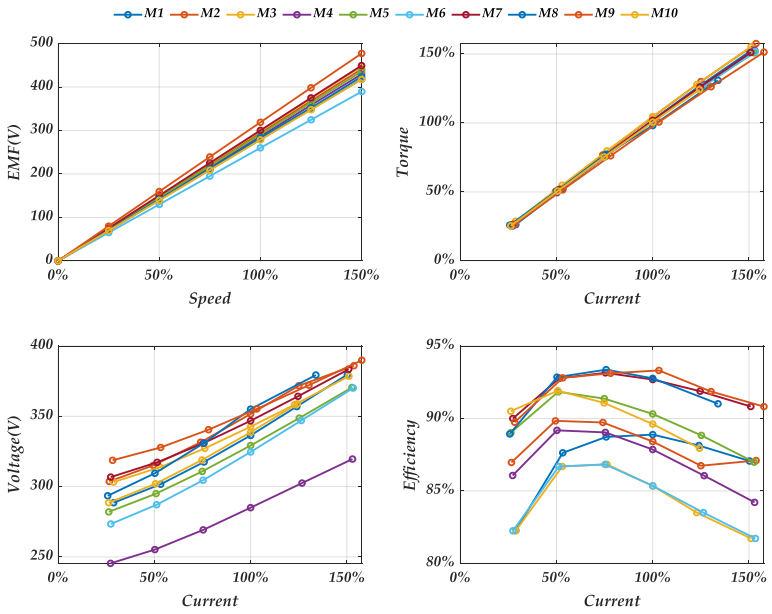

Figure 13. EMF, Torque, Voltage, and Efficiency vs. Current calculated by the Sizing Tool during the sizing process of 10 machines.

With respect to time consumption, sizing a machine with the proposed sizing tool takes less than one minute for each machine. Taking into account that sizing a machine with the classical method can take about 8 h, the time reduction is considerable. Naturally, obtaining magnetic flux and temperature maps takes time, but these calculations are carried out only once, so this time is paid off when some machines are sized.

With respect to the mapping process, the computation of a temperature map with a resolution of 13 stack length values, 15 Joule loss values, and 15 Magnetic loss values could take around 2 h. This leads to a 3D matrix with $13 \times 15 \times 15$ dimensions. Magnetic flux map creation for six temperatures varying i_q with 10 values over a full electric cycle takes approximately 6 h, but, applying the 1/6 reduction mentioned in Section 2, the consumed time is reduced in a 83%, leading to a 6×10 2D Matrix.

3.4. Experimental Validation

As the final step of the designing process, all sized machines are prototyped and experimentally tested to validate the designs. The test bench is shown in Figure 14.

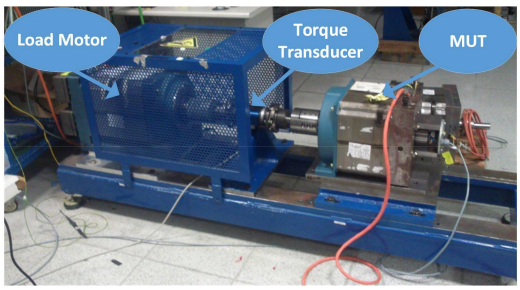

Figure 14. Picture of the test bench consisting of the load motor, the motor under test (MUT), and the torque transducer.

In Figure 15, the main experimental performances, such as electromotive force, torque, supplying voltage, and efficiency are shown for all built prototypes.

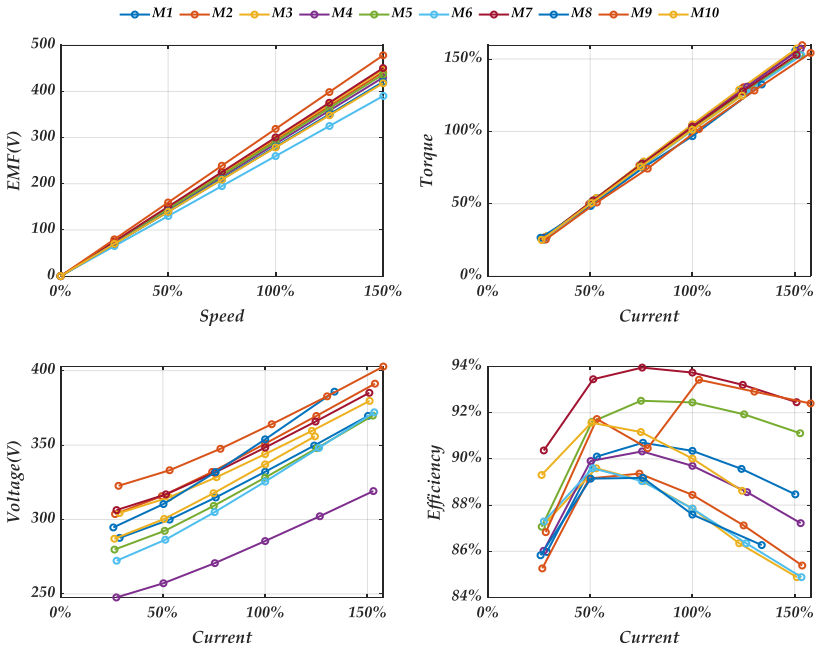

Figure 15. Experimental results of EMF, Torque, Voltage, and Efficiency vs. Current measured during the validation tests of the 10 sized motors.

As illustrated in the upper-left of Figure 15, speed and EMF are proportional and most of the machines have a similar k_e. In the bottom-left side, voltage is plotted against the current, and the majority of the machines follow a similar trend, although the values differ slightly. With respect to the efficiency, on the bottom-right side, it can be seen that efficiency decreases in low and high currents, and it increases in medium and nominal currents.

To validate the accuracy of the proposed sizing tool, the obtained results during the sizing process are compared to the experimental measurements. In Figure 16, the difference between sizing tool results and experimental results is plotted for the 10 sized motors.

It can be seen that the maximum difference in the EMF is about 1%, whereas, in the supplying voltage, it is about 2%. Nevertheless, the mean error is about 0.2% and 0.5%, respectively. With respect to the torque, the maximum difference is about 5% at low currents, mainly due to the uncertainty in the measurements at low currents. Nevertheless, it must be emphasized that the error is rather small as it is below 1.5%.

Then, in Figure 17, the results of a given machine, the M7 (see Table 1), are shown for a close-up view. As illustrated in Figure 17, measurements agree with the sizing tool results with a small difference at some points.

Concerning the efficiency, higher differences can be observed. This could be due to many different factors—on one hand, due to the uncertainty in the calculation of iron losses, mechanical losses, and stray losses; on the other hand, due to the possible measuring errors in the torque transducer and Voltage/Current probes. Even these errors might not be very significant, as it is shown in the torque comparison; for instance, the accumulation of all of them could justify the differences in the efficiency. In any case, it must be stated that these differences are not very significant, as the error is very low, below 6%.

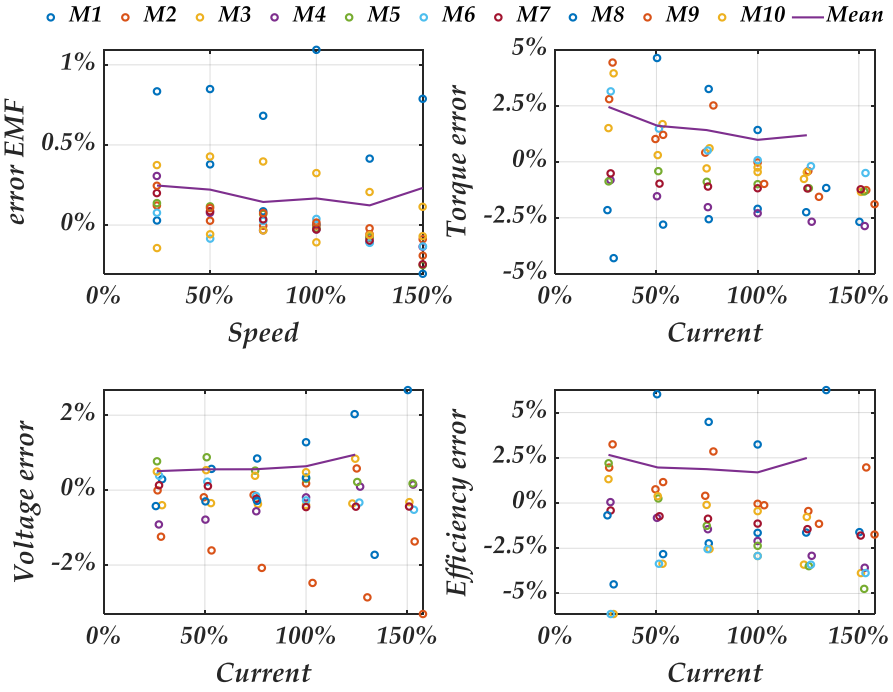

Figure 16. Error of the sizing tool computed as the difference in percentage between the experimental measurements and the results given by the sizing tool; error computed for the 10 sized motors.

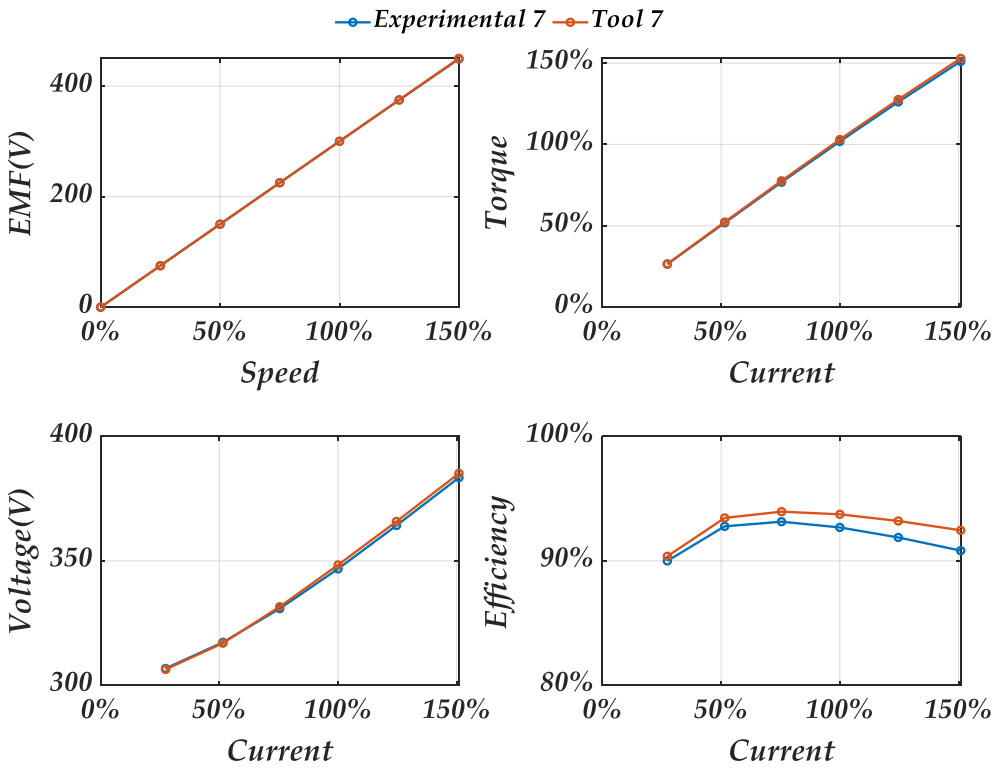

Figure 17. Comparison between experimental and calculated results in the M7 motor.

4. Conclusions

In this paper, a PM machines sizing methodology is developed. The proposed methodology, based on the coupling of magnetic flux and temperature maps, has been put into practice in a real case study. This methodology improves the competitiveness of ten industrial motors, reducing the design time and, consequently, the resources needed for that design. As a result, all motors have been sized accomplishing a very good trade-off between cost and required performances.

This procedure enables to perform sizing in a faster way, using less computational resources. Using magnetic flux and temperature maps enables achieving very good accuracy. As the influence of the temperature is considered, the accomplished results are more realistic. It must be remarked that specialized software is only needed for Map creation, and the sizing algorithm can be run on any computer.

Moreover, a faster procedure is described to obtain magnetic flux maps at different temperatures, just simulating 1/6 portion of the electric period, instead of considering the overall electric period. This method makes it possible to reduce the mapping process time in 83%.

Taking the overall results into account, the proposed sizing method fulfills the desired objectives of time reduction and accuracy in the sizing process, coupling electromagnetic with thermal effects, and sizing machines in less than a minute and with an error below 6%.

Author Contributions: G.A., A.E., and A.J.E. conceptualized the research; A.E. and Y.M. developed the methodology and the software; P.M. conceived and performed the experiments; P.M. and G.A. analyzed the data; Y.M. wrote the original draft; All authors have revised, edited, and approved the manuscript.

Funding: This research received no external funding.

Conflicts of Interest: The authors declare no conflict of interest.

Abbreviations

The following abbreviations and symbols are used in this manuscript:

CAD	Computer Aided Design
CFD	Computational Fluid Dynamics
FEA	Finite-Element analysis
GUI	Graphic User Interface
LP	Lumped Parameter
LPC	Lumped Parameter Circuit
PMSM	Permanent Magnet Synchronous Machines

List of symbols

$\overrightarrow{A}$	Magnetic vector complexpotential (Wb/m)	p_{Fe}	Core loss per weight (W/kg)
A_r	Copper wire Area (m^2)	p_h	Hysteresis loss per weight (W/kg)
α	Steinmetz coefficient	P_{LCu}	Joule Losses (W)
B_{si}	i^{th} harmonic amplitude of the stator flux density (T)	P_{Lmag}	Magnetic Losses (W)
D	Stator Diameter (m)	$\varphi_{d,q}$	Magnetic Flux of d,q axis (Wb)
f	Frequency (Hz)	φ_a	Magnetic Flux A (Wb)
$i_{d,q}$	d,q axis current (A)	φ_b	Magnetic Flux B (Wb)
I_n	Desired nominal current (A)	φ_c	Magnetic Flux C (Wb)
k_a	Empirical coefficient	Q_s	Number of slots in the stator
k_c	Eddy current loss coefficient	R_{Cu}	Winding Resistance (Ω)
k_e	Excess loss coefficient	ρ	Wire resistivity (Ωm)
k_f	Filling factor	$[\sigma]$	Tensor of the conductivity of the medium (S)
k_h	Hysteresis loss coefficient	T_{Cu}	Copper Temperature (° C)
k_{ov}	Overlapping factor	T_{magnet}	Magnet Temperature (° C)
L	Machine stack length (m)	T_{nom}	Nominal Torque (Nm)
L_{end}	End-Winding length (m)	V	Electric scalar potential (V)

L_{ini}	Estimated initial machine stack length (m)	$[v_0]$	Reluctivity of the vacuum (m/H)
L_σ	Leakage inductance (H)	$[v_\mathrm{r}]$	Tensor of the reluctivity of the medium
L_q	Q axis inductance (H)	$V_\mathrm{d,q}$	d,q axis voltage (V)
N	Winding number of turns	V_max	Maximum allowed voltage (V)
N_ini	Estimated initial winding number of turns	w_e	Machine rotational speed (rad/s)
n_cap	Winding layers	W_m	Weight of motor (kg)
p	Machine pole pairs	w_s	Slot width (m)
p_c	Eddy current loss per weight (W/kg)	Z	Number of conductors per slot
p_e	Excess loss per weight (W/kg)		

References

1. Hoang, K.D.; Atallah, K. Rapid sizing concept of interior permanent magnet machine for traction applications. *J. Eng.* **2019**, *2019*, 3956–3961, doi:10.1049/joe.2018.8169.
2. Zhou, K.; Pries, J.; Hofmann, H. Computationally Efficient 3D Finite-Element-Based Dynamic Thermal Models of Electric Machines. *IEEE Trans. Transp. Electrif.* **2015**, *1*, 138–149, doi:10.1109/TTE.2015.2456429.
3. Goss, J.; Wrobel, R.; Mellor, P.; Staton, D. The design of AC permanent magnet motors for electric vehicles: A design methodology. In Proceedings of the 2013 IEEE International Electric Machines and Drives Conference, IEMDC 2013, Chicago, IL USA, 12–15 May 2013; pp. 871–878, doi:10.1109/IEMDC.2013.6556200.
4. Xie, P.; Ramanathan, R.; Vakil, G.; Gerada, C. Simplified analytical machine sizing for surface mounted permanent magnet machines. In Proceedings of the 2019 IEEE International Electric Machines and Drives Conference, IEMDC 2019, San Diego, CA, USA, 12–15 May 2019; pp. 751–757, doi:10.1109/IEMDC.2019.8785167.
5. Wang, Y.; Bonfante, M.; Bianchi, N.; Petrella, R. Scalability of Synchronous Reluctance Machines Considering Thermal Performance. In Proceedings of the 2019 IEEE Energy Conversion Congress and Exposition (ECCE), Baltimore, MD, USA, 29 September–3 October 2019; pp. 1701–1707.
6. Tiegna, H.; Amara, Y.; Barakat, G. Overview of analytical models of permanent magnet electrical machines for analysis and design purposes. *Math. Comput. Simul.* **2013**, *90*, 162–177, doi:10.1016/j.matcom.2012.12.002.
7. Amrhein, M.; Krein, P.T. Magnetic equivalent circuit simulations of electrical machines for design purposes. In Proceedings of the IEEE Electric Ship Technologies Symposium, ESTS 2007, Arlington VA, USA, 21–23 May 2007; pp. 254–260, doi:10.1109/ESTS.2007.372095.
8. Zhou, K.; Ivanco, A.; Filipi, Z.; Hofmann, H. Finite-Element-Based Computationally Efficient Scalable Electric Machine Model Suitable for Electrified Powertrain Simulation and Optimization. *IEEE Trans. Ind. Appl.* **2015**, *51*, 4435–4445, doi:10.1109/TIA.2015.2451094.
9. Ramakrishnan, K.; Stipetic, S.; Gobbi, M.; Mastinu, G. Optimal Sizing of Traction Motors Using Scalable Electric Machine Model. *IEEE Trans. Transp. Electrif.* **2018**, *4*, 314–321, doi:10.1109/TTE.2017.2750488.
10. Carbonieri, M.; Bianchi, N.; Alberti, L. Induction Motor Mapping Using Rotor Field-Oriented Analysis Technique. In Proceedings of the 2019 IEEE Energy Conversion Congress and Exposition (ECCE), Baltimore, MD, USA, 29 September–3 October 2019; pp. 2321–2328.
11. Boglietti, A.; Cavagnino, A.; Staton, D.; Shanel, M.; Mueller, M.; Mejuto, C. Evolution and modern approaches for thermal analysis of electrical machines. *IEEE Trans. Ind. Electron.* **2009**, *56*, 871–882, doi:10.1109/TIE.2008.2011622.
12. Huang, Z.; Márquez-Fernández, F.J.; Loayza, Y.; Reinap, A.; Alaküla, M. Dynamic thermal modeling and application of electrical machine in hybrid drives. In Proceedings of the 2014 International Conference on Electrical Machines, ICEM 2014, Berlin, Germany, 2–5 September 2014; Institute of Electrical and Electronics Engineers Inc.: Piscataway, NJ, USA, 2014; pp. 2158–2164, doi:10.1109/ICELMACH.2014.6960483.
13. Li, J.; Ni, J.; Xu, X. *Lumped Parameter Transient Thermal Model of Motor Considering Temperature and Flow Rate of Cooling Water*; SAE Technical Papers; SAE International: Warrendale, PA, USA, 2019; Volume 2019, doi:10.4271/2019-01-0890.
14. Kral, C.; Haumer, A.; Lee, S.B. A practical thermal model for the estimation of permanent magnet and stator winding temperatures. *IEEE Trans. Power Electron.* **2014**, *29*, 455–464, doi:10.1109/TPEL.2013.2253128.

15. Sciascera, C.; Giangrande, P.; Papini, L.; Gerada, C.; Galea, M. Analytical thermal model for fast stator winding temperature prediction. *IEEE Trans. Ind. Electron.* **2017**, *64*, 6116–6126, doi:10.1109/TIE.2017.2682010.
16. Mondal, D.; Chakrabarti, A.; Sengupta, A.; Mondal, D.; Chakrabarti, A.; Sengupta, A. Fundamental Models of Synchronous Machine. In *Power System Small Signal Stability Analysis and Control*; Academic Press: Cambridge, MA, USA, 2014; Chapter 2, pp. 15–40, doi:10.1016/B978-0-12-800572-9.00002-0.
17. Yanli, F.; Chengning, Z. *Analytical Calculation for Predicting the Core Loss of Surface-Mounted Permanent Magnet Machine*; Energy Procedia; Elsevier Ltd.: Amsterdam, The Netherlands, 2017; Volume 105, pp. 2119–2124, doi:10.1016/j.egypro.2017.03.595.